PHYSICAL REVIEW D **76,** 016001 (2007)

CP asymmetry in charged Higgs decays in the MSSM

Mariana Frank* and Ismail Turan†

Department of Physics, Concordia University, 7141 Sherbrooke Street West, Montreal, Quebec, Canada H4B 1R6

(Received 21 March 2007; published 3 July 2007)

We discuss and compare the charge-parity (CP) asymmetry in the charged Higgs boson decays $H^- \to \bar{u}_i d_j$ for the second and third generation quarks in the minimal supersymmetric standard model. As part of the analysis, we derive some general analytical formulas for the imaginary parts of two-point and three-point scalar one-loop integrals and use them for calculating vectorial- and tensorial-type integrals needed for the problem under consideration. We find that, even though each decay mode has a potential to yield a CP asymmetry larger than 10%, further analysis based on the number of required charged Higgs events at colliders favors the $\bar{t}b$, $\bar{c}b$, and $\bar{c}s$ channels, whose asymmetry could reach 10%–15% in certain parts of the parameter space.

DOI: 10.1103/PhysRevD.76.016001 PACS numbers: 11.30.Er, 12.60.Jv, 14.80.Cp

I. INTRODUCTION

Discrete charge-parity (CP) symmetry violation is an interesting and puzzling phenomenon within the standard model (SM). While the SM has been successful in explaining all of the available experimental data, it fails to provide an explanation for the breaking of CP. Insight into understanding its nature and structure would shed light on diverse issues ranging from the origin of the mass to the evolution of our Universe.

The SM presents an economical scenario for CP violation, described through only one weak phase in the Cabibbo-Kobayashi-Maskawa (CKM) matrix. Even though the observed direct CP violation in K [1] and B [2] decays can be accommodated via the CKM matrix of the SM, this is not true for other phenomena, such as the matter-antimatter asymmetry present in the Universe. In addition, the standard model fails to explain the origin of CP violation but merely parametrizes it. Thus the SM framework could be viewed as a low energy effective version of a more complete theory, and CP violation offers a motivation to go beyond the SM. In the models beyond the SM, the existence of new sources of CP violation other than the CKM phase resolves some of the problems of the SM, but not all. One of the leading candidates of physics beyond the SM is supersymmetry, in particular, the minimal supersymmetric standard model (MSSM). Supersymmetry provides a compelling argument for the stabilization of the Higgs sector against quadratic divergencies and allows unification of gauge couplings at high energies, both unexplained by the SM. In the MSSM, enough baryon asymmetry can be generated at the electroweak scale at any temperature by means of the existence of an additional Higgs doublet. However, the MSSM has difficulty reconciling the smallness of the electric dipole moments with expectations of scalar fermion masses and the size of new CP violating phases introduced by soft supersymmetry breaking [3].

In the MSSM, there are many parameters which can, in principle, be complex, even after making all allowed rotations to get rid of unphysical phases. This raises the interesting possibility that CP violation, or CP asymmetries, might arise in other sectors of the model than the quark sector, and that would provide a spectacular signal of physics beyond the standard model. In particular, it is possible that there might be a close relationship between the Higgs sector and CP violation. The structure and properties of the Higgs sector are under intense scrutiny at present. Though indications at CERN LEP for a light Higgs boson of mass around 115 GeV are encouraging, they await confirmation.

Searching for Higgs bosons is one of the major objectives of present and future high energy experiments. In particular, a charged Higgs boson, predicted by most models to have mass of the order of the weak scale, would be a definite sign for physics beyond the SM. The phenomenology of charged Higgs bosons is less model dependent than that of neutral Higgs bosons, and it is governed by the values of $\tan\beta$ and $m_{H^\pm}$. Because charged Higgs couplings are proportional to fermion masses, the decays to third generation quarks and leptons are dominant. At hadron colliders, such as the Fermilab Tevatron and the CERN Large Hadron Collider (LHC), a light charged Higgs boson can be produced from the decay of the top quark via $t \to H^+ b$, if $m_{H^\pm} < m_t - m_b$. If the charged Higgs boson is heavier than the top quark, there are three channels for producing charged Higgs pairs: $pp \to H^+H^-$, $pp \to W^\pm H^\mp$, and $gb \to tH^-$; as well as the single charged Higgs production $\bar{c}s$, $\bar{c}b \to H^-$; see [4] and references therein. In many cases complementary information from more than one channel will be accessible at the LHC. The LHC has a high potential for detecting heavy Higgs states which might lie beyond the kinematic reach of the planned International Linear Collider (ILC). At the ILC, the main production mechanism for charged Higgs bosons would be

*mfrank@alcor.concordia.ca
†ituran@physics.concordia.ca

$e^+e^- \to H^+H^-$, followed by one of the allowed decays $H^+ \to t\bar{b}$, $\tau\nu_\tau$, or $c\bar{s}$. The pair production cross section for charged Higgs at ILC is about 2.5 times larger than for the neutral ones [5]. Provided that a Higgs boson couples to the Z boson, the ILC will observe it independently of its decay characteristics. The discovery potential is practically independent of $\tan\beta$ and extends up to 1.2 TeV for an integrated luminosity of 3000 fb^{-1} [5]. For specific examples of how the integrated information obtained by ILC and LHC can be used for Higgs detection and determination of parameters in the Higgs sector, see [6].

In its most general form, the MSSM predicts a plethora of new CP phases. These new sources of flavor and CP violation give rise to the enhancement of CP violation effects alluded to before, which could provide distinguishing signs for the MSSM at present and future colliders. In this study, we concentrate on the analysis of the CP asymmetry in charged Higgs decays $H^- \to \bar{u}_i d_j$ in the framework of the MSSM. Here $\bar{u}_i d_j = \bar{c}b$, $\bar{c}s$, $\bar{t}b$, $\bar{t}s$. The corresponding neutral Higgs CP asymmetry in $h \to d_i\bar{d}_j$ has been discussed in Ref. [7]. The CP asymmetry in the main decay mode $H^- \to \bar{t}b$ and other two-body nonquark charged Higgs decays have been considered in [8,9]. Recently, these authors have discussed various CP asymmetries in $H^- \to \bar{t}b$ by including the decay products of the top quark and subsequently the W boson and showed that the decay rate CP asymmetry can go up to 25% [10]. In this work, we revisit the asymmetries in $H^- \to \bar{t}b$, but also discuss the other three quark decay modes and compare the size of the CP asymmetry in all the channels. We show that, even though in some part of the parameter space the $\bar{t}s$ channel has sizable CP asymmetry with respect to the $\bar{t}b$, $\bar{c}b$, or $\bar{c}s$ channel, this result has to be taken with caution since the former has very small branching ratios (Br's) which makes it harder to observe it. We introduce and discuss another relevant quantity[1] [11], $(A_{CP}^2 \times \mathrm{Br})^{-1}$, for each decay mode, with A_{CP} the CP asymmetry and Br the branching ratio for a given decay mode. This function was shown to be a measure of the number of required charged Higgs bosons to be produced at colliders for observing an asymmetry for a given channel. Based on this analysis, we conclude that $H^- \to \bar{c}b$, $H^- \to \bar{c}s$, and $H^- \to \bar{t}b$ are all optimal channels which could reveal a measurable CP asymmetry at the order of 10%–15%. We also discuss the CP asymmetry induced by the phases of the flavor violating parameters $\delta^{23}_{U,D}$ alone and note that their contribution is small and thus unlikely to account for a measurable CP asymmetry in any of the decay modes considered in this study.

The outline of the paper is as follows. In the next section, we briefly review the MSSM, concentrating on the sources of CP violation. The decay processes are presented in Sec. III and the numerical analysis of the decays under consideration in Sec. IV. We conclude in Sec. V. Details of the method used for calculations are presented in the Appendix.

[1] $(A_{CP}^2 \times \mathrm{Br})^{-1}$ is closely related to the total number of events N required to establish a measurable CP violation for a particular mode. The exact formula is $N = s^2(A_{CP}^2 \times \mathrm{Br}\epsilon)^{-1}$. Here s is the standard deviation and ϵ is the detection efficiency.

II. THE UNCONSTRAINED MINIMAL SUPERSYMMETRIC STANDARD MODEL

The superpotential $\mathcal{W}$ of the MSSM Lagrangian and the relevant part of the soft breaking Lagrangian $\mathcal{L}_{\mathrm{soft}}^{\mathrm{squark}}$ are, respectively,

$$\mathcal{W} = \mu H^1 H^2 + Y_l^{ij} H^1 L^i e_R^j + Y_d^{ij} H^1 Q^i d_R^j + Y_u^{ij} H^2 Q^i u_R^j, \tag{2.1}$$

$$\mathcal{L}_{\mathrm{soft}}^{\mathrm{squark}} = -\tilde{Q}^{i\dagger}(M_{\tilde{Q}}^2)_{ij}\tilde{Q}^j - \tilde{u}^{i\dagger}(M_{\tilde{U}}^2)_{ij}\tilde{u}^j - \tilde{d}^{i\dagger}(M_{\tilde{D}}^2)_{ij}\tilde{d}^j + Y_u^i A_u^{ij}\tilde{Q}_i H^2 \tilde{u}_j + Y_d^i A_d^{ij}\tilde{Q}_i H^1 \tilde{d}_j, \tag{2.2}$$

where H^1 and H^2 are the Higgs doublets with vacuum expectation values v_1 and v_2, respectively; Q is the $SU(2)$ scalar doublet; u, d are the up- and down-quark $SU(2)$ singlets, respectively; $\tilde{Q}$, $\tilde{u}$, $\tilde{d}$ represent scalar quarks; $Y_{u,d}$ are the Yukawa couplings; and i, j are generation indices. Here A^{ij} represent the trilinear scalar couplings. In Eq. (2.2) we are assuming a chiral limit of the MSSM.

We work in the unconstrained version of the MSSM and use the mass eigenstate method [12], where squark mass matrices are given in the super-CKM basis and are diagonalized by rotating the superfields. In this basis, the up-squark and down-squark mass matrices are correlated by this rotation and thus not independent. Potential new sources of flavor violation arise from couplings of quarks and squarks to gauginos. This method has the advantage that, when the off-diagonal elements in the squark mass matrices become large, the method is still valid, unlike perturbation-based expansions. The up(down)-squark mass matrices between second and third generations are taken as

$$\mathcal{M}^2_{\tilde{u}\{\tilde{d}\}} = \begin{pmatrix} M^2_{\tilde{L}c\{s\}} & (M^2_{\tilde{U}\{\tilde{D}\}})_{LL} & m_{c\{s\}}\mathcal{A}_{c\{s\}} & (M^2_{\tilde{U}\{\tilde{D}\}})_{LR} \\ (M^2_{\tilde{U}\{\tilde{D}\}})_{LL} & M^2_{\tilde{L}t\{b\}} & (M^2_{\tilde{U}\{\tilde{D}\}})_{RL} & m_{t\{b\}}\mathcal{A}_{t\{b\}} \\ m_{c\{s\}}\mathcal{A}_{c\{s\}} & (M^2_{\tilde{U}\{\tilde{D}\}})_{RL} & M^2_{\tilde{R}c\{s\}} & (M^2_{\tilde{U}\{\tilde{D}\}})_{RR} \\ (M^2_{\tilde{U}\{\tilde{D}\}})_{LR} & m_{t\{b\}}\mathcal{A}_{t\{b\}} & (M^2_{\tilde{U}\{\tilde{D}\}})_{RR} & M^2_{\tilde{R}t\{b\}} \end{pmatrix} \tag{2.3}$$

with

$$\begin{aligned} M^2_{\tilde{L}q} &= M^2_{\tilde{Q},q} + m_q^2 + \cos 2\beta(T_q - Q_q s_W^2)M_Z^2, \\ M^2_{\tilde{R}\{c,t\}} &= M^2_{\tilde{U},\{c,t\}} + m^2_{c,t} + \cos 2\beta Q_t s_W^2 M_Z^2, \\ M^2_{\tilde{R}\{s,b\}} &= M^2_{\tilde{D},\{s,b\}} + m^2_{s,b} + \cos 2\beta Q_b s_W^2 M_Z^2, \\ \mathcal{A}_{c,t} &= A_{c,t} - \mu\cot\beta, \qquad \mathcal{A}_{s,b} = A_{s,b} - \mu\tan\beta, \end{aligned} \tag{2.4}$$

where we assume a general flavor violation among families. In addition to the flavor dependence in Yukawa matrices, there are additional sources of flavor violation due to the soft mass terms and A-terms. The richness of the flavor structure depends on the assumed textures of soft mass and A-terms at the grand unified theory (GUT) scale. Assuming both the soft mass and A-terms to be flavor blind at the GUT scale can still induce flavor violation at the electroweak scale due to their evolution from the GUT scale down to the electroweak scale using the renormalization group equations. The flavor violating effects become much bigger if the soft mass and/or A-term(s) are flavor dependent at the GUT scale (see, for example, [13] for details).

For reasons we discuss further on, we assume μ real and a common phase for $A_{c,t}$ and $A_{s,b}$. Note that A_s has a negligible effect since it is multiplied by the strange quark mass. Tanβ is the ratio of the vacuum expectation values of the two neutral Higgs bosons.

From the mass matrix, Eq. (2.3), we also define the flavor mixing parameters as scaled off-diagonal flavor violating entries

$$(\delta^{ij}_{U(D)})_{AB} = \frac{(M^2_{\tilde{U}(\tilde{D})})^{23}_{AB}}{M^2_{\rm SUSY}}, \qquad (A, B = L, R), \tag{2.5}$$

where $M_{\rm SUSY}$ is the common scale for the parameters $M^2_{\tilde{Q},q}$ and $M^2_{\tilde{U}(\tilde{D}),q}$. As mentioned before we allow $\delta^{23}_{U(D)}$'s to be complex (to have CP violating phases).

We do not repeat listing the chargino and neutralino sectors of the MSSM here, as we do not assume a new nonzero CP phase in either sector; for the details see Ref. [14]. As the gluino contribution is dominant for the charged Higgs decays, we give the relevant up-type quark-squark-gluino interaction $\tilde{g}$:

$$\begin{aligned}\mathcal{L}_{u\tilde{u}\tilde{g}} = \sum_{i=1}^{3} \sqrt{2}\, g_s T^r_{st}[\bar{u}^s_i (\Gamma_U)^{ia} P_L \tilde{g}^r \tilde{u}^t_a \\ - \bar{u}^s_i (\Gamma_U)^{(i+3)a} P_R \tilde{g}^r \tilde{u}^t_a + \text{H.c.}],\end{aligned} \tag{2.6}$$

where T^r are the $SU(3)_c$ generators, $P_{L,R} \equiv (1 \mp \gamma_5)/2$, $i = 1, 2, 3$ is the generation index, $a = 1, \ldots, 6$ is the scalar quark index, and s, t are color indices. There is a similar interaction for the down case.

Considering the number of complex parameters in the MSSM, further assumptions are needed for simplicity and predictability. In the gaugino sector, two of the three gaugino masses could be complex, unless a degenerate spectrum at the GUT scale is assumed. We assume all three gaugino mass terms real at any scale. The Higgsino mass parameter μ is, in principle, complex. However, the phase of μ is strongly constrained by the electron dipole moment (EDM) measurements of the neutron [15] and cannot exceed values of the order of 0.01–0.001. For the effects of CP violating SUSY phases on other EDMs and systems, see [16]. We simply neglect this phase and consider μ real. In the squark sector, there are trilinear soft couplings of quarks, $A_{u,d}$, which are complex. In addition to these, the misalignment between quarks and squarks arising through the diagonalization of their respective mass matrices leads to new sources of flavor violation, with parameters denoted as $\delta_{U,D}$. These are also generally complex and could have large imaginary parts. We will assume nonzero flavor violation only between the second and third generations, because the ones involving the first generation are required to be small, based on experimental constraints in K and D physics [13,17]. The kaon mass splitting parameter ΔM_K due to $K - \bar{K}$ mixing, and the parameters ϵ and ϵ' put severe constraints on the real and imaginary parts of the flavor violating parameters δ^{12}_D, respectively. Somewhat weaker bounds can also be obtained from K physics for the up sector between the first and second generations as well but stringent bounds on δ^{12}_U can be obtained by using the experimental bound on the $D - \bar{D}$ mixing parameter ΔM_D. In a similar fashion, the flavor violating parameters δ^{13}_D between the first and third generations can be restricted with the use of low energy B physics measurements (ΔM_{B_d}, $B \to X_s\gamma$, $S_{B\to\psi K_s}$). The common feature of these constraints is that the upper bounds on the flavor parameters involving the first generation have to be less than 0.1 [13,17]. There are however no similar limits on the mixings between the second and third generations so we will keep them arbitrary.

We assume that there are nonzero phases from the trilinear couplings $A_{u,d}$ and intergenerational flavor mixing parameters $\delta^{23}_{U,D}$. For further simplification, we assume a common phase $\arg[A_u] = \arg[A_d] \equiv \arg[A]$.

Thus, the supersymmetric sources of CP violation of interest in charged Higgs decays come from the soft broken terms $M^2_{\tilde{Q}}$, $M^2_{\tilde{U}}$ and the trilinear scalar coupling A_u, and are introduced through the matrix Γ_U. In the following section, we analyze their effects on the calculation of the CP asymmetry.

III. CHARGED HIGGS DECAYS $H^- \to \bar{u}_i d_j$

In this section we discuss the CP asymmetry in the charged Higgs boson decays $H^- \to \bar{u}_i d_j$, which is defined as[2]

$$A_{CP} = \frac{\Gamma(H^- \to \bar{u}_i d_j) - \Gamma(H^+ \to u_i \bar{d}_j)}{\Gamma(H^- \to \bar{u}_i d_j) + \Gamma(H^+ \to u_i \bar{d}_j)}, \tag{3.1}$$

where Γ is the partial decay width of the decay mode considered. These decays are tree-level processes and one could calculate the branching ratios, decays widths, etc. with tree-level approximation.

However, it is known that [18] the CP-odd observable A_{CP} requires a nontrivial phase from Feynman diagrams

[2]This type of CP asymmetry is sometimes called *partial rate asymmetry*. For other types see [10,18].

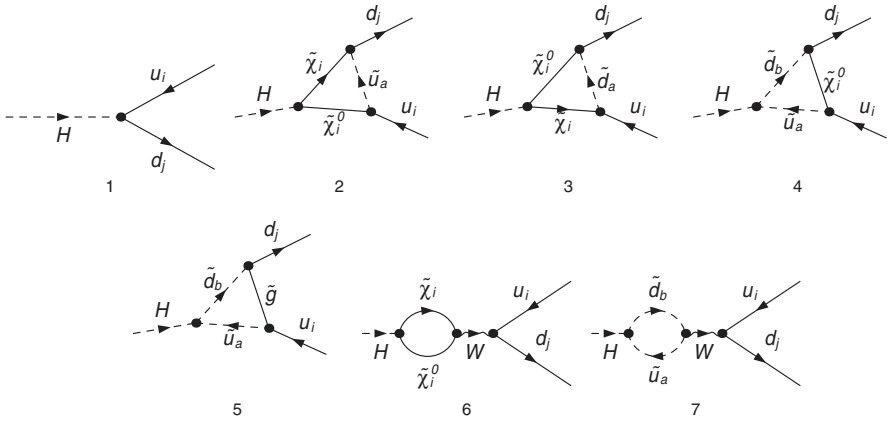

FIG. 1. The tree and relevant one-loop diagrams contributing CP asymmetry for the decays $H^- \to \bar{u}_i d_j$.

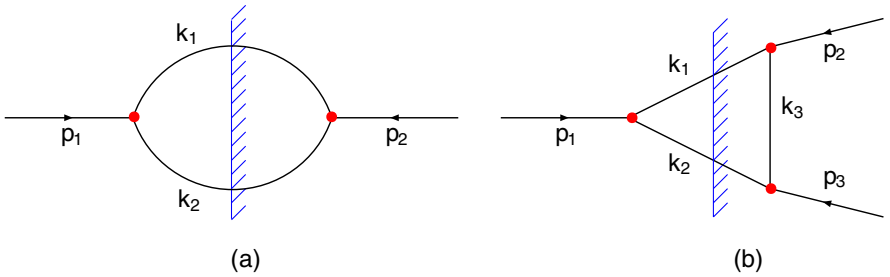

FIG. 2 (color online). The unitarity cuts for self-energy (a) and vertex-type (b) generic diagrams.

(called absorptive or strong phase), in addition to the weak phase mentioned in the previous section. This way, the imaginary part of the amplitude is nonzero, Im(amplitude) $\neq 0$. One way of introducing such a phase is through one-loop Feynman diagrams, where some of the intermediate particles go on shell. Then, the numerator of Eq. (3.1) will be proportional to the interference term between tree-level and one-loop contributions. The tree-level and relevant one-loop contributions to the decays $H^- \to \bar{u}_i d_j$ are shown in Fig. 1.

There are many more one-loop contributions to the decays, but based on various kinematical considerations only six of them are relevant to A_{CP} (four vertex-type and two self-energy–type diagrams).[3] We consider cuts through chargino-neutralino internal lines, or through up-squark–down-squark lines. We will call them *internal-cut* states. They contribute to the CP asymmetry when $m_H \geq m_{\tilde{\chi}^0} + m_{\tilde{\chi}^+}$ and $m_H \geq m_{\tilde{u}} + m_{\tilde{d}}$ are satisfied, so that the chargino and the neutralino can go on shell. This is the necessary condition to induce an absorptive part into the amplitude. The generic self-energy and vertex-type diagrams with cuts are shown in Fig. 2 where the *internal-cut* states represent two possibilities in each case. Here we do not count the flipping cases ($k_1 \leftrightarrow k_2$), which are only relevant to the vertex-type diagrams, in which case the third intermediate state is different. For the vertex-type diagrams, Fig. 2(b), there are two other possible cuts, through $k_1 - k_3$ or $k_2 - k_3$. The cut with $k_1 - k_3$ is not kinematically allowed since it requires $m_{d_j} \geq m_{\tilde{d}_a} + m_{\tilde{\chi}_n^0}$, $m_{d_j} \geq m_{\tilde{d}_a} + m_{\tilde{\chi}_c^+}$, or $m_{d_j} \geq m_{\tilde{d}_a} + m_{\tilde{g}}$. None of these conditions is possible.

For the case with the $k_2 - k_3$ cut, based on the current experimental bounds on the mass of the lightest neutralino and the lightest up-type squarks, there could be some contributions to the decay mode $H^- \to \bar{t} d_j$ from diagrams (2) and (4) of Fig. 1 in a very narrow kinematical range ($m_{\tilde{u}} + m_{\tilde{\chi}^0} \lesssim m_t$). We simply neglect such contributions. There exists yet another way to produce the necessary absorptive cut, by taking the invariant mass squared for the final states, $(p_2 + p_3)^2$, to be greater than $(m_{\tilde{\chi}^0} + m_{\tilde{\chi}^+})^2$ which results in some cuts in the phase space. This method was pursued in [19], in the analysis of the three-body semileptonic top quark decays.

One can show that the numerator of Eq. (3.1) is proportional to the imaginary part of the amplitude from loop diagrams[4] arising from tree-level-loop interference terms.

[3]There exist additionally some SM vertex contributions with W bosons, CP-even Higgs bosons, and quarks in the loop. We do not get CP asymmetry contributions from such diagrams since we take μ real. For the case with complex μ, see [8].

[4]For example, see [18] for details.

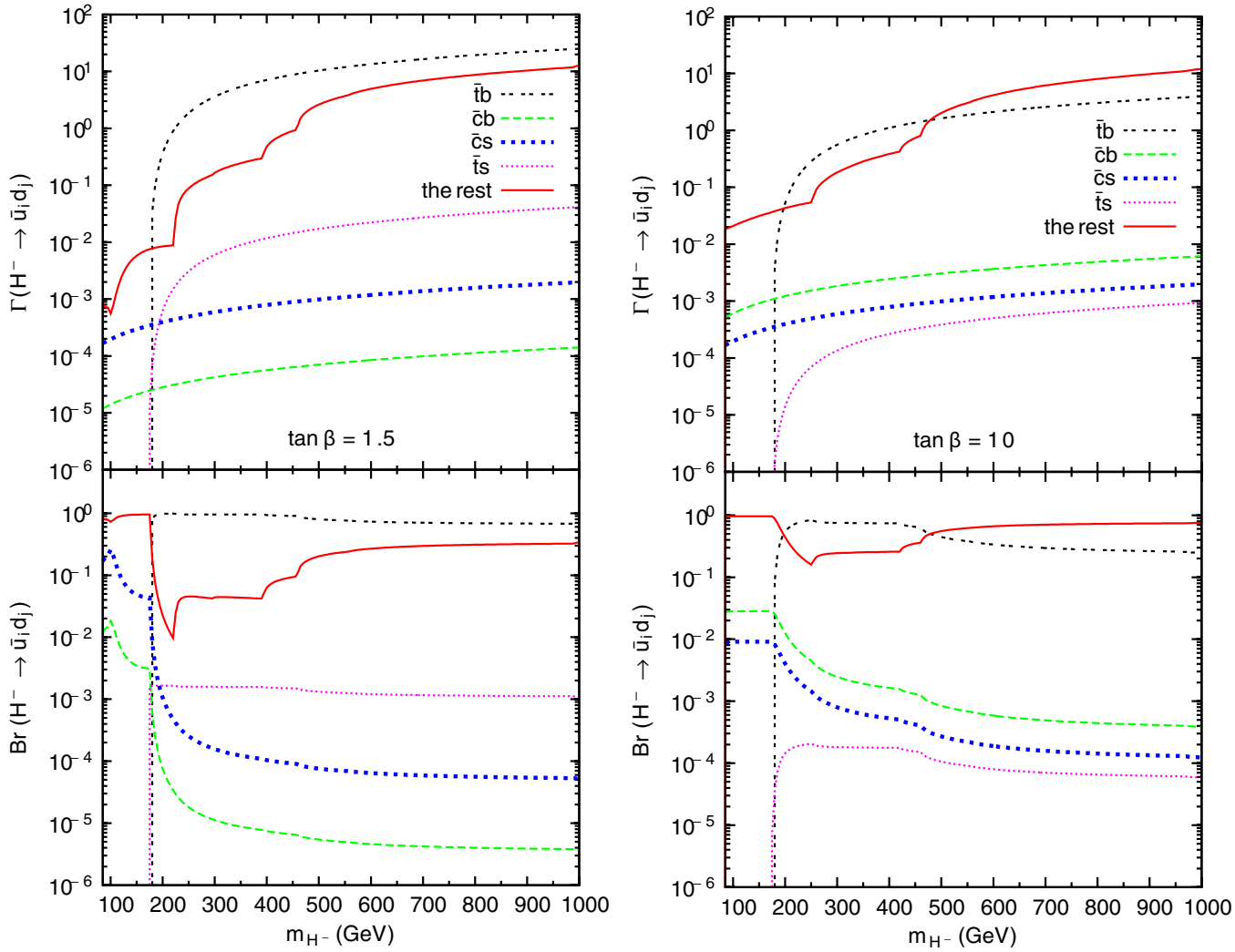

FIG. 3 (color online). The partial decay widths and branching ratios of the charged Higgs boson decays $H^- \to \bar{u}_i d_j$. For the supersymmetric channels, $M_1 = 95$ GeV, $M_2 = 200$ GeV, $\mu = 250$ GeV, $M_{\rm SUSY} = 500$ GeV, and $A = 400$ GeV.

As usual, we neglect possible loop-loop interference effects which are much smaller than tree-loop terms. In the Appendix, instead of giving rather lengthy analytical results for this imaginary part, we outline the method used to do the calculation using the cuts in Fig. 2. We present it in a generic way, valid for the four decay modes of the charged Higgs boson, $H^- \to \bar{u}_i d_j$.

IV. NUMERICAL ANALYSIS

In this section, we present comparatively our numerical results for the decays $H^- \to \bar{u}_i d_j (u_i = c, t, d_j = s, b)$.[5] In the calculation of the *CP* asymmetry from the formula in Eq. (3.1), we use the tree-level values instead of one loop when evaluating the sum of the partial decay widths (Γ) in the denominator, which simplifies the numerical calculations. This approximation is not valid for the numerator where one-loop contributions are needed to extract the *CP* phases.

In Fig. 3 we show the partial decay widths of the channels $H^- \to \bar{c}b$, $\bar{c}s$, $\bar{t}b$, $\bar{t}s$ at tree level, together with their branching ratios for small and intermediate tanβ values. We represent the other tree-level decay channels as "*the rest*" and we use the FEYNHIGGS program [20] to calculate the partial decay widths of these channels. Basically, depending on the charged Higgs mass, "*the rest*" includes the lepton channels $H^- \to e\nu_e$, $\mu\nu_\mu$, $\tau\nu_\tau$; the neutralino-chargino channels $H^+ \to \chi_i^+ \chi_j^0$, $i = 1, 2$, $j = 1, \ldots, 4$; the Higgs-vector boson channels $H^\pm \to h^0 W$, $H^0 W$, $A^0 W$; and the sfermion channels $H^\pm \to \tilde{f}_i \tilde{f}_j$ $i, j = 1, \ldots, 3$. Inclusion of these channels is important as

[5]The *CP* asymmetry in one of these decays, $H^- \to \bar{t}b$, has been discussed in [8] under a different parameter set and with different assumptions. A good agreement is obtained once we switch our parameter values to their set.

it affects the number of charged Higgs bosons required to observe the asymmetry, as discussed later in this section.

In the region $m_{H^+} \geq m_t$, $H^- \to \bar{t}b$ is the dominant mode. However, in the region $m_{H^+} \leq 140$ GeV, the leptonic decay $H^\pm \to \tau\nu_\tau$ becomes the main decay channel, and in between these regions, including threshold effects, the below-threshold three-body decay $H^\pm \to hW^*$ has a branching ratio comparable to, or even dominating over, other channels, its exact value depending on the mixing in the Higgs sector. Inclusion of threshold effects also opens other three-body channels, like $H^\pm \to A^0 W^*$ and $H^- \to b\bar{t}^*$ that have sizable branching ratios in the intermediate mass range. We do not include the threshold effects, but see [21] for details. We note that, for heavy charged Higgs, the neutralino-chargino channels are comparable with the $\bar{t}b$ channel. However, it is important to observe that, among these decays, $H^- \to \bar{c}s$ and $H^- \to \bar{c}b$ have non-negligible branching ratios. This is important for our analysis, since observability of CP asymmetry in a specific channel requires not only a sizable asymmetry but also an experimentally viable branching ratio. We must comment on the strange quark mass dependence: as seen from Fig. 3, while the partial decay widths for $\bar{t}b$ and $\bar{t}s$ channels are suppressed as $\tan\beta$ gets larger, the opposite is true for the $\bar{c}b$ channel. This is due to the fact that, evaluating the Feynman diagrams in Fig. 1, the scalar quark couplings to the charged Higgs are proportional to $(m_u \cot\beta + m_d \tan\beta)$, as seen from Eq. (2.3). There is no suppression in the $\bar{c}s$ curve since for intermediate $\tan\beta$ values the term proportional to the strange quark mass is comparable to the one with the charm quark mass and becomes dominant for larger $\tan\beta$ values. So, one must keep the strange quark mass nonzero, at least for $\bar{c}s$ decay. Of course, its effect in the $\bar{t}s$ case is negligible.

For the numerical analysis, we fix some of the parameters of the model globally because the CP asymmetry is not very sensitive to their variations. As mentioned before, we introduce a common phase and magnitude for the trilinear couplings A_u and A_d as $\arg[A]$ and A. The Higgs parameter μ is taken real. We allow the gluino mass $m_{\tilde{g}}$ to be light. We also use the parametrization for squark mass matrices where a common scale $M_{\rm SUSY}$ is chosen for the soft breaking parameters $M^2_{\tilde{Q},q}$ and $M^2_{\tilde{U}(\tilde{D}),q}$. The flavor violating parameters (δ's) are set to zero everywhere except for the case where we test the sensitivity of A_{CP} to these parameters. There exist two other free parameters in the Higgs sector of the MSSM, taken in a popular framework to be $\tan\beta$, and one of the Higgs boson masses, often taken as the CP-odd Higgs mass m_{A^0}. Of course we could equally well assume any of the others as the free Higgs mass parameter. As it is more convenient for the present analysis, we choose m_{H^+} as the free Higgs mass here. Unless otherwise stated, we fix the following parameters globally,[6]

$$M_{\rm SUSY} = 500 \text{ GeV}, \quad \mu = 250 \text{ GeV}, \quad \tan\beta = 10, \quad M_2 = 200 \text{ GeV}, \quad m_{\tilde{g}} = 250 \text{ GeV}. \tag{4.1}$$

In Fig. 4 we illustrate the dependence of the CP asymmetry A_{CP} on the phase $\arg[A]$ for each decay for a variety of A values. As expected, the behavior is periodic and the sensitivity to both $\arg[A]$ and A is quite significant. It seems that each decay mode can have an asymmetry as large as 10%–15%. It is also seen that the asymmetry produced in $H^- \to \bar{c}s$ and $H^- \to \bar{t}s$ decay modes could be comparable to or even larger than $H^- \to \bar{c}b$ or $H^- \to \bar{t}b$. Of course this is not very unusual, since it is possible to get large asymmetries for decays with smaller branching ratios [18]. Therefore, determining the optimum channel among these decays requires further analysis, but qualitatively one can predict that $H^- \to \bar{c}b$ and $H^- \to \bar{t}b$ have similar asymmetries. The $\bar{c}b$ mode has non-negligible branching ratios due to the fact that CKM suppression is compensated by the large m_b mass appearing in the couplings. In the parameter space that we explore, the diagrams with a chargino-neutralino/neutralino in the loop give negligible results compared to the gluino loop diagrams. So, the main contribution comes from the gluino vertex diagram (diagram 5 of Fig. 1), while the self-energy diagram (diagram 7 of Fig. 1) is also important. We keep these contributions, but include and check the others wherever relevant.

Additionally, we want to test whether it is possible to account for a sizable asymmetry in charged Higgs decays by introducing complex flavor mixing parameters between second and third generation quarks and keeping all the other parameters real. This is a secondary effect since, unlike the case with nonzero phase $\arg[A]$, getting the absorptive phase through such parameters requires not only a chirality flip in the squark propagators but also a mass insertion for flavor changing as well (this is a CP breaking and flavor violating effect). In Fig. 5 we show the asymmetry A_{CP} as a function of the phase $\arg[(\delta^{23}_U)_{LL}]$ for various charged Higgs masses. The small graphs inside each graph represent the positive asymmetry A_{CP} in the logarithmic scale, so that one can distinguish the curves with different charged Higgs masses. With the exception of the $H^- \to \bar{c}b$ decay mode, which can have as large as 0.3% CP asymmetry for $m_{H^+} = 300$ GeV, the other decays yield negligible asymmetries. The absolute value of $(\delta^{23}_U)_{LL}$ is set to 0.5, but A_{CP} is not very sensitive to the value of this parameter. We also checked the asymmetry induced by the phases of the other δ parameters in both the up and down sectors, but they all give negligible contributions. Therefore, it is unlikely that a measurable CP asymmetry in charged Higgs decays $H^- \to \bar{u}_i d_j$ is generated only by an absorptive phase from $(\delta^{23}_U)_{LL}$.

In the next two figures, Figs. 6 and 7, we plot the CP asymmetry A_{CP}, for various $\arg[A]$ values, as a function of

[6]The gluino mass is consistent with Tevatron limits [1].

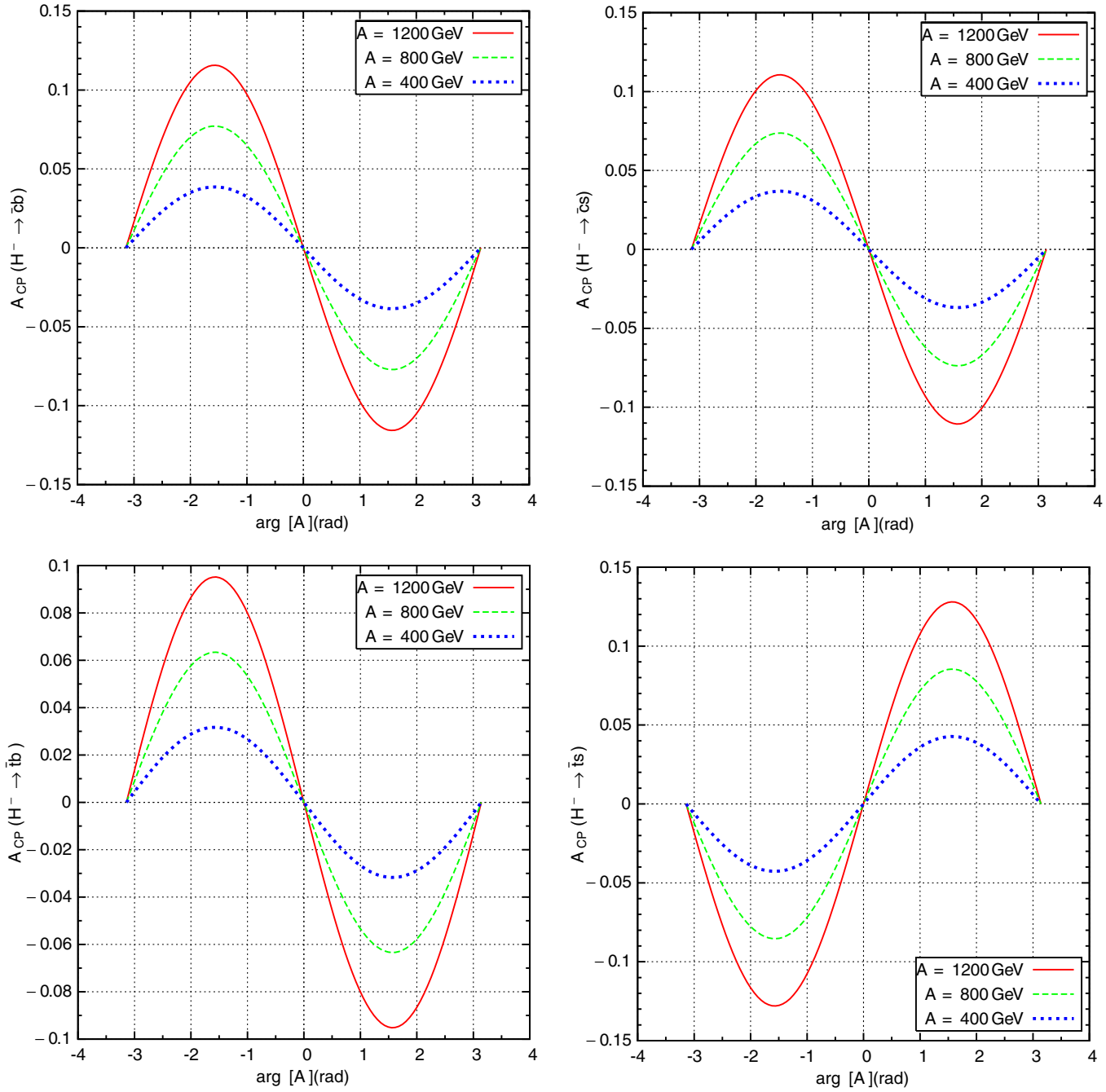

FIG. 4 (color online). The *CP* asymmetry for the charged Higgs decays $H^- \to \bar{u}_i d_j$ as a function of the phase arg$[A]$ for the various values of A.

A and the gluino mass $m_{\tilde{g}}$, respectively. A_{CP} in both of the decays $H^- \to \bar{c}b$ and $H^- \to \bar{c}s$ in Fig. 6 can be as large as 14% at arg$[A] = \pi/2$ for large A values, but $H^- \to \bar{t}b$ remains slightly smaller. The *CP* asymmetry in $H^- \to \bar{t}s$ becomes even bigger, but this has to be taken with some care. More than 10% asymmetry could be achieved for each decay mode for $A = 1200$ GeV and if the gluino is very light (~ 200 GeV), as shown in Fig. 7. We note that there exists similar dependence on the charged Higgs mass. The *CP* asymmetry also changes between $\pm 15\%$ as we vary $\tan\beta$. The dependence is significant especially for light charged Higgs masses and small $\tan\beta$ values.

In order to test the viability of these channels for the search of *CP* asymmetry, we scanned the parameter space spanned by the most sensitive decay channels and compared the number of events (which can be taken as the required number of charged Higgs bosons) as a function of $(A_{CP}^2 \times \mathrm{Br})^{-1}$. In Fig. 8, we show the scatter plots

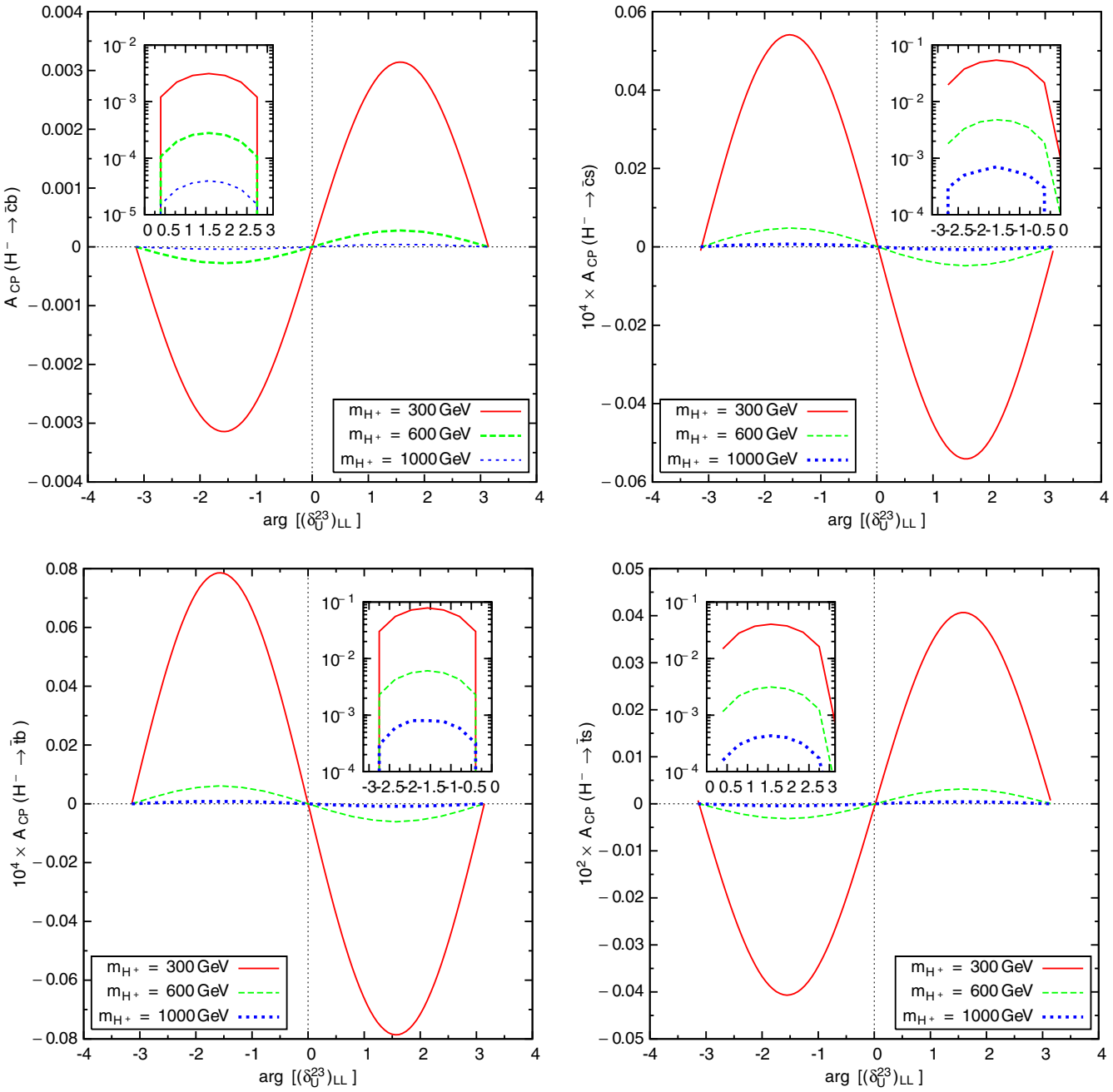

FIG. 5 (color online). The same as Fig. 4 but as a function of the phase of the flavor violating parameter $\arg[(\delta_U^{23})_{LL}]$ for various m_{H^+} values. We take $A = 1200$ GeV and $\arg[A] = 0$. The absolute value of $(\delta_U^{23})_{LL}$ is set to 0.5. The small graphs inside each graph represent the positive asymmetry A_{CP} in the logarithmic scale.

for the charged Higgs decays $H^- \to \bar{u}_i d_j$ in the $(A_{CP}^2 \times \mathrm{Br})^{-1} - A_{CP}$ plane. These events are obtained by running the sensitive parameters randomly in the parameter ranges $A \in (0, 1400)$ GeV, $\arg[A] \in (-\pi, \pi)$, $m_{\tilde{g}} \in (200, 1000)$ GeV, $m_{H^+} \in (200, 1000)$ GeV, and $\tan\beta \in (1, 50)$. Note that the x axes are in the logarithmic scale. The branching ratios are calculated by evaluating all the other tree-level charged Higgs decay widths with the FEYNHIGGS program. Again, the small graphs show the positive part of the asymmetry distribution in the logarithmic scale. From these scatter plots, one can make a few observations.

Each decay channel has a possibility to develop an asymmetry bigger than 10%. In the case of $H^- \to \bar{c}s$ and $H^- \to \bar{t}s$, there are quite a number of events which yield asymmetries around 15%, which is as large an asymmetry

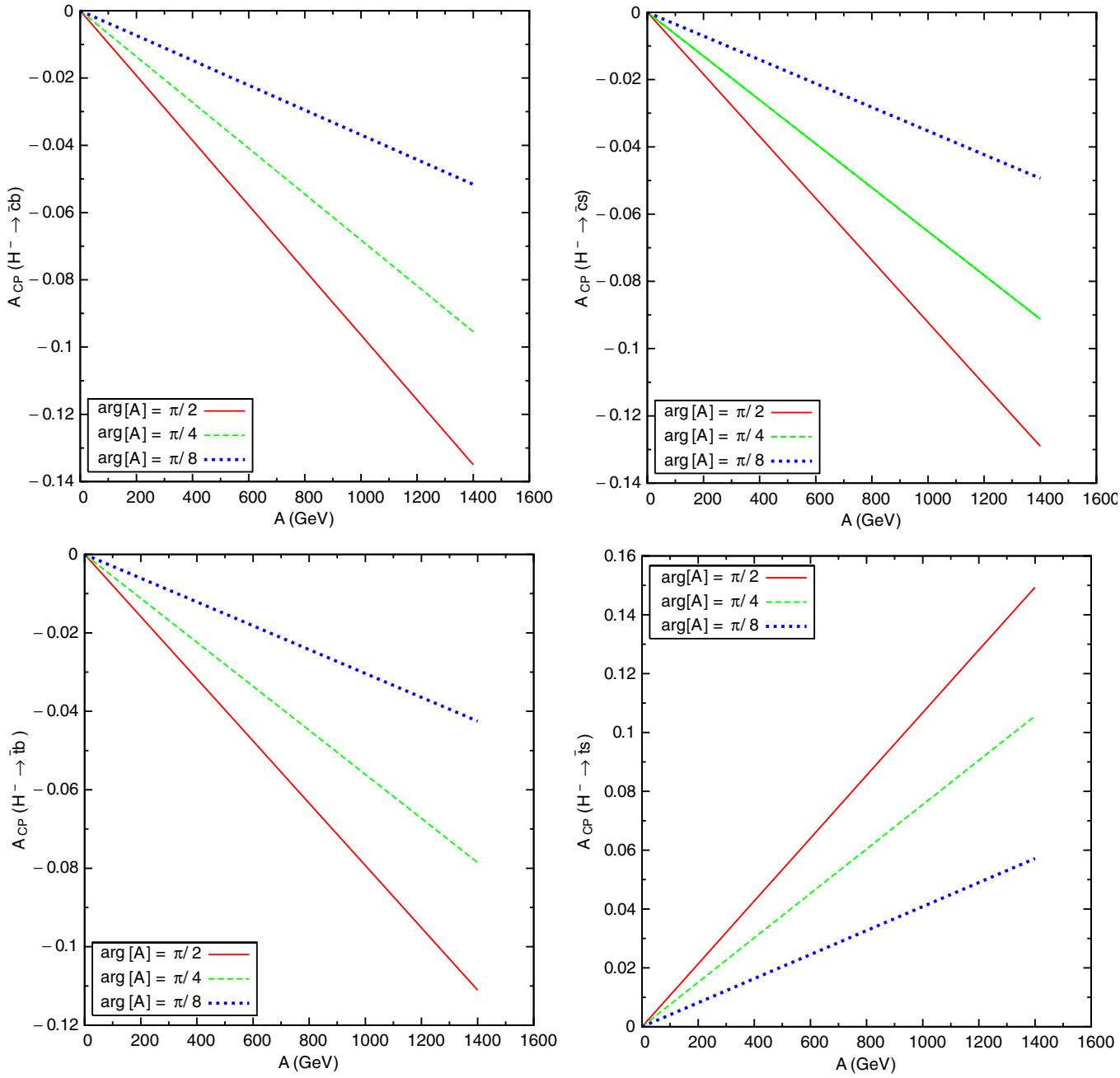

FIG. 6 (color online). The *CP* asymmetry for the charged Higgs decays $H^- \to \bar{u}_i d_j$ as a function of A for the various values of the phase arg$[A]$.

as the other two channels can attain. But the number of charged Higgs bosons required to observe such an asymmetry is around 10^5–10^6 for $\bar{t}s$ decay, which is 2 to 4 orders of magnitude more than the number needed to make such a measurement in the $H^- \to \bar{c}b$ or $H^- \to \bar{t}b$ channel, respectively. On the other hand, $H^- \to \bar{c}s$ yields a comparable asymmetry distribution with respect to $H^- \to \bar{c}b$, and also the required number of charged Higgs is similar for some part of the parameter space which maximizes the asymmetry. Clearly, the parameter set for the maximal scenario is different for each decay mode. Such a similarity between $\bar{c}s$ and $\bar{c}b$ channels is not surprising since the $\bar{c}s$ decay mode can have a branching ratio comparable to, or larger than, that of the $\bar{c}b$ decay mode, depending on the value of $\tan\beta$. In the $\bar{c}s$ channel, since the strange quark is light, it is difficult to distinguish it from the $\bar{c}d$ channel.

So, we can conclude that, depending mainly on the $\tan\beta$ value, the asymmetry in both $\bar{c}b$ and $\bar{c}s$ can be competitive with the one from $\bar{t}b$ if there are enough charged Higgs bosons produced at the colliders. But one needs at least 10^2

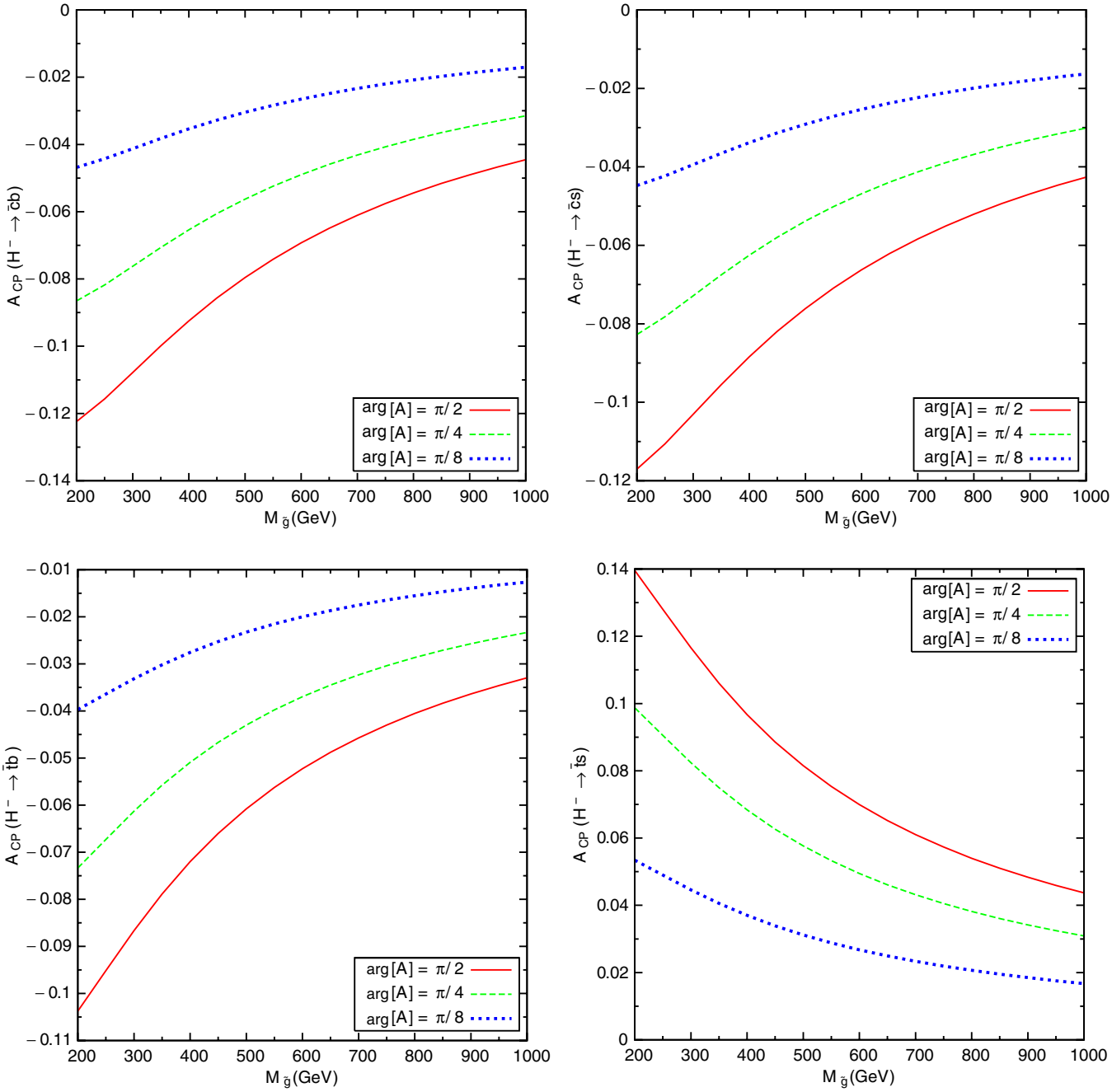

FIG. 7 (color online). The same as Fig. 6 but as a function of the gluino mass $m_{\tilde{g}}$. $A = 1200$ GeV is assumed.

times more statistics for the $\bar{c}b$ and $\bar{c}s$ cases. From Fig. 8, the distribution of the events for $\bar{t}b$ modes, unlike the other channels, is not scattered much since, in almost the entire parameter range considered in the scan, its branching ratio remains constant.

In the last figure, Fig. 9, we perform the same scan of the parameter space as before, but with a nonzero phase $\arg[(\delta_U^{23})_{LL}]$ in the up-type squark mixing matrix, while switching the phase of A off. So, instead of running the trilinear coupling A and its phase, we run $(\delta_U^{23})_{LL}$ and its phase in the range (0, 0.5) and $(-\pi, \pi)$, respectively. It seems that the largest asymmetry comes from the $H^- \to \bar{c}b$ process which could be at most as large as 0.6%–0.8%, but at least 10^6 Higgs must be produced to probe such an asymmetry. Additionally, the asymmetry is still significantly smaller than the case where the absorptive phase originated from the trilinear couplings. For the other channels, not only are the asymmetries very small, but as a consequence the number of charged Higgs required to observe them is enormous.

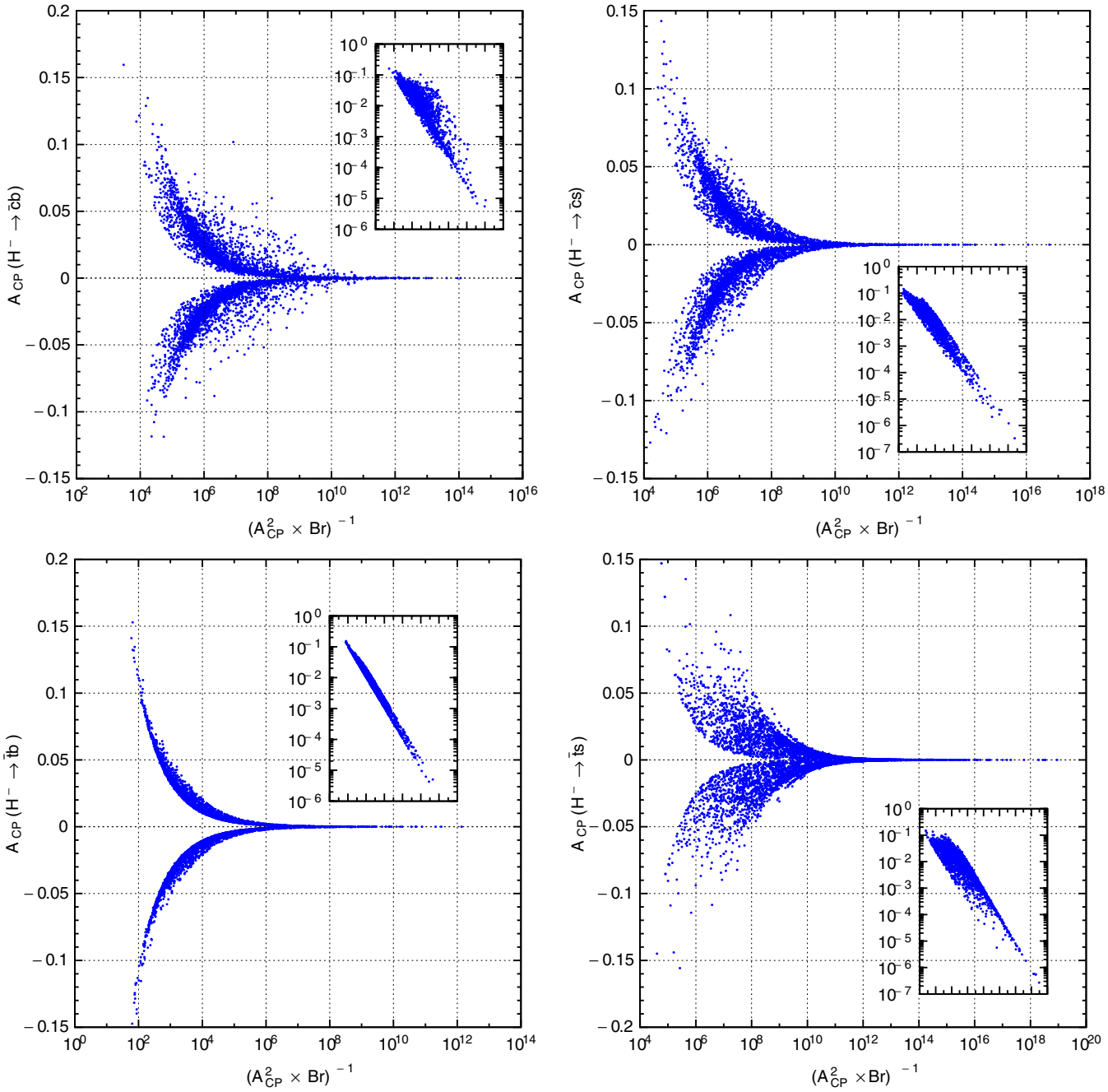

FIG. 8 (color online). The scatter plots for the charged Higgs decays $H^- \to \bar{u}_i d_j$ in the $(A_{CP}^2 \times \mathrm{Br})^{-1} - A_{CP}$ plane. These are obtained by scanning the sensitive parameters $A \in (0, 1400)$ GeV, $\arg[A] \in (-\pi, \pi)$, $m_{\tilde{g}} \in (200, 1000)$ GeV, $m_{H^+} \in (200, 1000)$ GeV, and $\tan\beta \in (1, 50)$. The x axes are in the logarithmic scale. The small graphs inside each graph represent the positive asymmetry A_{CP} in the logarithmic scale.

V. SUMMARY AND CONCLUSION

In this study, we analyzed the possibility of obtaining measurable signals for *CP* asymmetry in the charged Higgs decays $H^- \to \bar{u}_i d_j$ for the second and third generation quarks in the MSSM. Above the top quark threshold, charged Higgs bosons decay mainly to $\bar{t}b$, but decays to $\bar{c}b$, $\bar{c}s$, and $\bar{t}s$ are also relevant. The *CP* asymmetry of the main decay mode $\bar{t}b$ and other nonquark charged Higgs decays have been considered previously [8–10]. Here we analyzed, discussed, and compared all significant quark channels to pinpoint which one is more likely to produce a visible asymmetry at the colliders. A nonzero *CP* asymmetry requires an absorptive phase, for which we considered possible interference terms between tree-level and one-loop diagrams. Then we calculated the imaginary parts

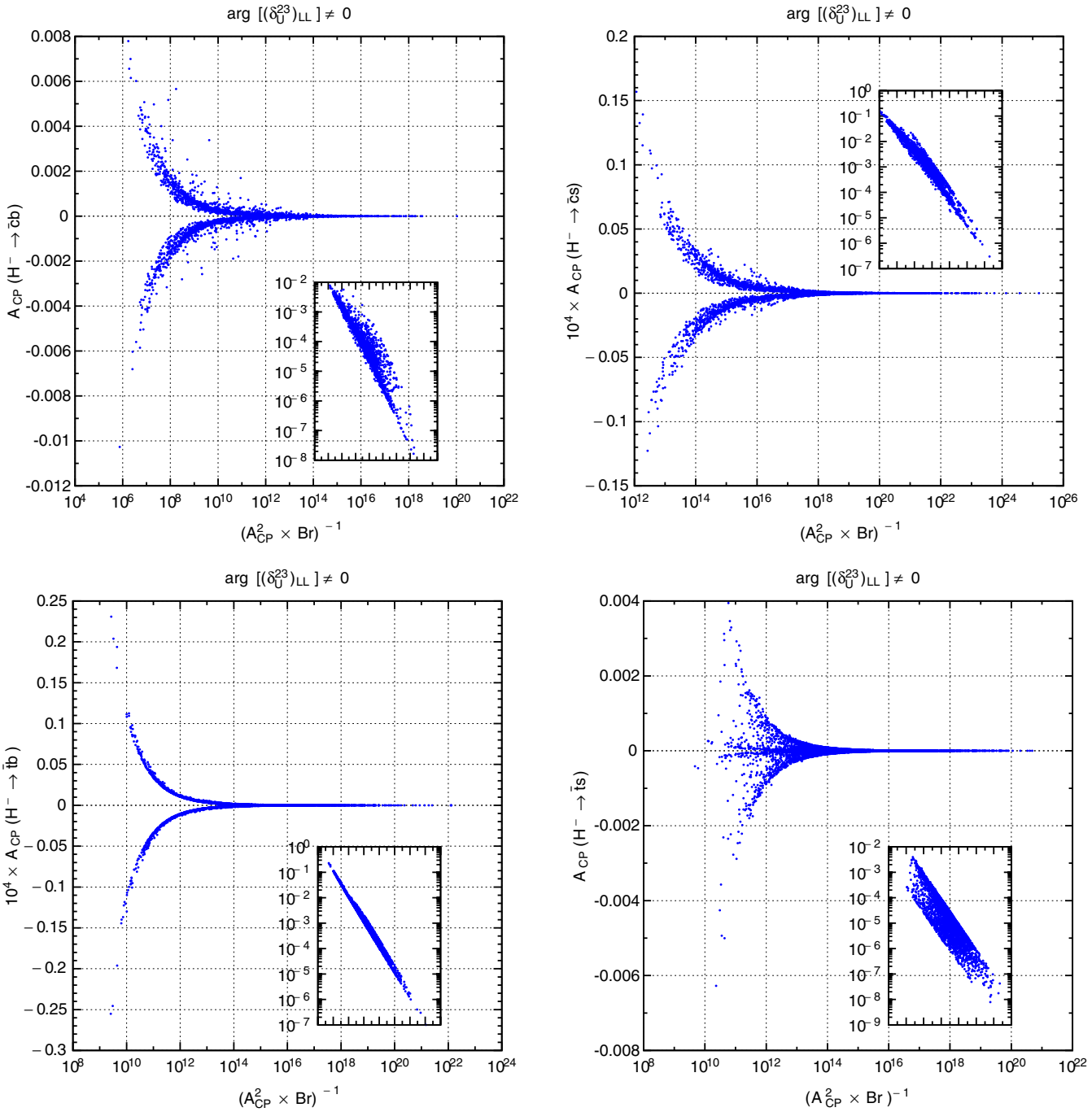

FIG. 9 (color online). The same as Fig. 8 but for the nonzero arg$[(\delta_U^{23})_{LL}]$ phase. A is set to 1200 GeV and taken real. The x axes are in the logarithmic scale. The small graphs inside each graph represent the positive asymmetry A_{CP} in the logarithmic scale.

of scalar two- and three-point functions of the one-loop diagrams by first deriving generic analytical formulas for the discontinuity in such diagrams with the help of Cutkosky rules. We then presented the results obtained for the vectorial and tensorial types of integrals. Within the MSSM framework, we investigated the effect on the asymmetry of two relevant absorptive phases: the common phase of the trilinear couplings A and the phase of the flavor violating parameter $(\delta_U^{23})_{LL}$. We analyzed their effects separately and without considering any interference effects.

Consideration of nonzero values for arg$[A]$ predicted asymmetries around 10%–15% for each decay mode. However, by including the requirement that $(A_{CP}^2 \times \mathrm{Br})^{-1}$ is proportional to the number of required Higgs bosons, our analysis indicates that only $H^- \to \bar{t}b$ and

$H^- \to \bar{c}b$, $\bar{c}s$ decay processes would be likely to induce a measurable *CP* asymmetry, with the requirement that at least 10^2–10^4 charged Higgs bosons be produced at the colliders. Unlike the phase arg$[A]$, the phase $(\delta_U^{23})_{LL}$ cannot account for a sizable *CP* asymmetry A_{CP}. In this case, only $H^- \to \bar{c}b$ can get an asymmetry around 0.6%–0.8%, with the requirement that 10^6 charged Higgs bosons must be produced at the colliders, in order to translate into a measurable asymmetry. The fact that the arguments of A and $(\delta_U^{23})_{LL}$ give rise to *CP* asymmetries of different orders of magnitude justifies *a posteriori* neglecting interference effects.

ACKNOWLEDGMENTS

This work is supported in part by NSERC of Canada under Grant No. SAP01105354.

APPENDIX: THE METHOD CALCULATION OF THE IMAGINARY PART

We calculate the absorptive part of the loop diagrams by applying the Cutkosky rules. In general, in the loop integration, we end up with a numerator with scalar, vectorial, or tensorial structures (and their pseudo counterparts), depending on the types of particles running in the loop. We first consider the scalar case and then outline the method for the vectorial and tensorial cases and present the results. We discuss self-energy and vertex cases separately.

1. Two-point function

In Fig. 2(a), if we assume that particles running in the loop are scalar, we get a B_0-type scalar two-point Passarino-Veltman function [22]. We use the convention that all external momenta are incoming and Fig. 2(a) can be expressed as

$$B_0(p^2, m_1^2, m_2^2) = \frac{i}{\pi^2}\int d^4k \frac{1}{(k^2 - m_1^2)((p-k)^2 - m_2^2)}, \tag{A1}$$

where m_1 and m_2 are the masses of the particles in the loop. By applying the Cutkosky rules [23] for Fig. 2(a) we have, for the discontinuity across this cut,

$$\begin{aligned}\Delta B_0(p_1^2, m_1^2, m_2^2) &= \frac{i}{\pi^2}\int d^4k_1 2\pi\Theta(k_1^0)\delta(k_1^2 - m_1^2) \\ &\quad \times 2\pi\Theta(p_1^0 - k_1^0)\delta((p_1 - k_1)^2 - m_2^2) \\ &= 2\pi i \frac{\sqrt{\lambda(p_1^2, m_1^2, m_2^2)}}{p_1^2} \\ &\quad \times \Theta(p_1^2 - (m_1 + m_2)^2),\end{aligned} \tag{A2}$$

where k_1^0 and p_1^0 are the energies of the corresponding particles. ΔB_0 represents the discontinuity of B^0 and is related to the imaginary part of the diagram up to a factor of $2i$ (see [24] for example). $\lambda(x, y, z)$ is the usual Källen function defined as $\lambda(x, y, z) = (x - y - z)^2 - 4yz$. The argument of the Heaviside function Θ in the final result ensures that both *internal-cut* states, particles 1 and 2, go on shell in the loop.

Now let us assume that we have a vectorial term in the numerator. If we denote this integral as B^μ, then the discontinuity can be written

$$\begin{aligned}\Delta B^\mu(p_1^2, m_1^2, m_2^2) &\equiv \Delta B_0(p_1^2, m_1^2, m_2^2) \otimes k^\mu \\ &= \begin{cases} \frac{p_1^2 + m_1^2 - m_2^2}{2\sqrt{p_1^2}} \Delta B_0(p_1^2, m_1^2, m_2^2) & \mu = 0, \\ 0 & \mu = i, \end{cases}\end{aligned} \tag{A3}$$

where "$\otimes k^\mu$" means that k^μ should be considered as a part of the integrand of the ΔB_0 term.

In a similar manner, one can calculate a tensorial type of two-point integral. Since we will need terms only up to second rank tensors in our calculation, it is enough to calculate $\Delta B^{\mu\nu}$ for the discontinuity in such cases, and the result can be expressed as

$$\begin{aligned}\Delta B^{\mu\nu}(p_1^2, m_1^2, m_2^2) &\equiv \Delta B_0(p_1^2, m_1^2, m_2^2) \otimes (k^\mu k^\nu) \\ &= \kappa^{\mu\nu}\Delta B_0(p_1^2, m_1^2, m_2^2),\end{aligned} \tag{A4}$$

where

$$\kappa^{\mu\nu} = \mathrm{Diag}\left(\kappa^0, \frac{\kappa}{3}, \frac{\kappa}{3}, \frac{\kappa}{3}\right), \qquad \kappa^0 = \frac{(p_1^2 + m_1^2 - m_2^2)^2}{4p_1^2}, \qquad \kappa = \frac{\lambda(p_1^2, m_1^2, m_2^2)}{4p_1^2}. \tag{A5}$$

Then the imaginary part of the self-energy diagrams shown in the last two graphs of Fig. 1 becomes the sum of the above terms,

$$\begin{aligned}\mathrm{Im\,(self\text{-}energy)} = \frac{1}{2i}\sum_l (&Y_l \Delta B_0 + Y_l^\mu \Delta B_\mu \\ &+ Y_l^{\mu\nu}\Delta B_{\mu\nu}),\end{aligned} \tag{A6}$$

where Y_l's include all other contributions arising from the Feynman rules and the index l runs over loop diagrams.

2. Three-point function

The evaluation is similar to the two-point function case but the calculation is more cumbersome. We first give the result for the discontinuity in a three-point scalar integral, known as $C_0(p_1^2, p_2^2, p_3^2, m_1^2, m_2^2, m_3^2)$.[7] Here $m_{1,2,3}$ are the internal masses. Again using Cutkosky rules, we have[8] for the discontinuity

[7]For simplicity, we suppress the argument of C_0 in the rest of the paper.

[8]Our result is consistent with the one given in [24].

$$\Delta C_0 = \frac{i}{\pi^2}\int d^4k_1 \frac{2\pi\Theta(k_1^0)\delta(k_1^2-m_1^2)2\pi\Theta(-p_2^0-p_3^0-k_1^0)\delta((p_2+p_3+k_1)^2-m_2^2)}{(p_3+k_1)^2-m_3^2}$$
$$= \frac{-2\pi i}{\sqrt{\lambda(p_1^2,p_2^2,p_3^2)}}\log\left(\frac{\alpha+\beta}{\alpha-\beta}\right)\Theta(p_1^2-(m_1+m_2)^2), \tag{A7}$$

where

$$\alpha = p_1^2(p_1^2+2m_3^2-(p_2^2+p_3^2+m_1^2+m_2^2)) - (m_1^2-m_2^2)(p_2^2-p_3^2),$$
$$\beta = \sqrt{\lambda(p_1^2,m_1^2,m_2^2)\lambda(p_1^2,p_2^2,p_3^2)}. \tag{A8}$$

The vectorial-type integrals can be calculated as follows. The extra term k_1^μ can be converted into the external momenta p_i's and their derivatives with the help of the propagator in the denominator [25]. For example,

$$\frac{k_1^\mu}{(p_3+k_1)^2-m_3^2} = \frac{1}{2}\frac{\partial}{\partial p_{3\mu}}[\log((p_3+k_1)^2-m_3^2)] - \frac{p_3^\mu}{(p_3+k_1)^2-m_3^2}. \tag{A9}$$

For convenience, we define $(p_3+k_1)^2-m_3^2 \equiv D$, $f_0 \equiv 1/D$, $f_1 \equiv \log(D)$, and $f_2 \equiv D(\log(D)-1)$. This way we can express the discontinuities in both the vectorial and the 2nd rank tensorial-type integrals in the following form:

$$\Delta C^\mu = -p_3^\mu \Delta C_0 + \frac{1}{2}\frac{\partial}{\partial p_{2\mu}}\Delta C_1, \qquad \Delta C^{\mu\nu} = p_3^\mu p_3^\nu \Delta C_0 - \frac{1}{2}\left(g^{\mu\nu} + p_3^\mu\frac{\partial}{\partial p_{2\nu}} + p_3^\nu\frac{\partial}{\partial p_{2\mu}}\right)\Delta C_1 + \frac{1}{4}\frac{\partial}{\partial p_{2\mu}}\frac{\partial}{\partial p_{2\nu}}\Delta C_2,$$
$$\Delta C_1 = \Delta C_0(f_0 \to f_1), \qquad \Delta C_2 = \Delta C_0(f_0 \to f_2). \tag{A10}$$

Then, computing ΔC_1 and ΔC_2 integrals in a straightforward manner, we find

$$\Delta C_1 = -\frac{\alpha+\beta}{2p_1^2}\Delta C_0 + \frac{2\pi i}{p_1^2}\sqrt{\lambda(p_1^2,m_1^2,m_2^2)}\log\left(\frac{\alpha-\beta}{2p_1^2 e}\right)\Theta(p_1^2-(m_1+m_2)^2),$$
$$\Delta C_2 = \frac{(\alpha+\beta)^2}{8p_1^4}\Delta C_0 - \frac{\pi\alpha i}{p_1^4}\sqrt{\lambda(p_1^2,m_1^2,m_2^2)}\log\left(\frac{\alpha-\beta}{2p_1^2 e^{3/2}}\right)\Theta(p_1^2-(m_1+m_2)^2). \tag{A11}$$

Here e is Napier's constant. Next, we take the derivatives of ΔC_1 and ΔC_2 with respect to $p_{2,3}$ and plug them into Eq. (A10). After some lengthy algebra, we get

$$\Delta C^\mu = \frac{2\pi i\Theta(p_1^2-(m_1+m_2)^2)}{\sqrt{\lambda(p_1^2,p_2^2,p_3^2)}}\left[\log\left(\frac{\alpha+\beta}{\alpha-\beta}\right)p_3^\mu - \left((u-\alpha v)\log\left(\frac{\alpha+\beta}{\alpha-\beta}\right)+2\beta v\right)\frac{p_2^\mu}{2p_1^2}\right],$$
$$\Delta C^{\mu\nu} = \frac{2\pi i\Theta(p_1^2-(m_1+m_2)^2)}{p_1^2\sqrt{\lambda(p_1^2,p_2^2,p_3^2)}}\left(\frac{g^{\mu\nu}}{2}\Delta C_g + \frac{p_2^\mu p_2^\nu}{8p_1^2}\Delta C_{22} + (p_2^\mu p_3^\nu + p_2^\nu p_3^\mu)\Delta C_{23} + p_3^\mu p_3^\nu \Delta C_{33}\right),$$
$$\Delta C_g = \frac{\alpha\beta v}{4p_1^2} - (\alpha+\beta)\left(\frac{1}{2} - \frac{u}{4p_1^2} + \frac{(\alpha-\beta)v}{8p_1^2}\right)\log\left(\frac{\alpha+\beta}{\alpha-\beta}\right) - \beta\left(1-\frac{u}{2p_1^2}\right)\log\left(\frac{\alpha-\beta}{2p_1^2 e}\right), \tag{A12}$$
$$\Delta C_{22} = \left[(\alpha^2-\beta^2)\left(\frac{1}{\lambda(p_1^2,p_2^2,p_3^2)} - v^2\right) - 2(u-\alpha v)^2\right]\log\left(\frac{\alpha+\beta}{\alpha-\beta}\right) + 8\beta v(u-\alpha v) + 2\alpha\beta\left(\frac{1}{\lambda(p_1^2,p_2^2,p_3^2)} + v^2\right),$$
$$\Delta C_{23} = \beta v + \frac{u-\alpha v}{2}\log\left(\frac{\alpha+\beta}{\alpha-\beta}\right),$$
$$\Delta C_{33} = -p_1^2\log\left(\frac{\alpha+\beta}{\alpha-\beta}\right),$$

where $u = p_1^2 + m_1^2 - m_2^2$ and $v = (p_1^2 - p_2^2 + p_3^2)/\lambda(p_1^2,p_2^2,p_3^2)$ and $g^{\mu\nu} = (+,-,-,-)$ is the metric tensor.

It remains only to determine the coefficients, like the ones defined in Eq. (A6), by comparing the actual matrix elements for the diagrams in Fig. 1. The diagrams in Fig. 1 and the corresponding matrix elements are generated with the software FEYNARTS [26] and then we do the rest of the calculation with our own code.

[1] W. M. Yao *et al.* (Particle Data Group), J. Phys. G **33**, 1 (2006).
[2] B. Aubert *et al.* (*BABAR* Collaboration), Phys. Rev. D **65**, 091101 (2002); K. Abe *et al.* (Belle Collaboration), Phys. Rev. Lett. **87**, 091802 (2001).
[3] W. Buchmuller and D. Wyler, Phys. Lett. **121B**, 321 (1983); J. Polchinski and M. B. Wise, Phys. Lett. **125B**, 393 (1983); A. De Rujula, M. B. Gavela, O. Pene, and F. J. Vegas, Phys. Lett. B **245**, 640 (1990).
[4] S. Hao, M. Wen-Gan, Z. Ren-You, G. Lei, H. Liang, and J. Yi, Phys. Rev. D **75**, 095006 (2007).
[5] E. Coniavitis and A. Ferrari, Phys. Rev. D **75**, 015004 (2007).
[6] G. Weiglein *et al.* (LHC/LC Study Group), Phys. Rep. **426**, 47 (2006).
[7] D. A. Demir, Phys. Lett. B **571**, 193 (2003).
[8] E. Christova, H. Eberl, W. Majerotto, and S. Kraml, Nucl. Phys. **B639**, 263 (2002); **B647**, 359(E) (2002).
[9] E. Christova, H. Eberl, W. Majerotto, and S. Kraml, J. High Energy Phys. 12 (2002) 021; E. Christova, E. Ginina, and M. Stoilov, J. High Energy Phys. 11 (2003) 027.
[10] E. Christova, H. Eberl, E. Ginina, and W. Majerotto, J. High Energy Phys. 02 (2007) 075.
[11] G. Eilam, J. L. Hewett, and A. Soni, Phys. Rev. Lett. **67**, 1979 (1991).
[12] T. Besmer, C. Greub, and T. Hurth, Nucl. Phys. **B609**, 359 (2001); D. A. Demir, Phys. Lett. B **571**, 193 (2003); A. M. Curiel, M. J. Herrero, and D. Temes, Phys. Rev. D **67**, 075008 (2003); J. J. Liu, C. S. Li, L. L. Yang, and L. G. Jin, Nucl. Phys. **B705**, 3 (2005).
[13] P. H. Chankowski, O. Lebedev, and S. Pokorski, Nucl. Phys. **B717**, 190 (2005).
[14] M. Frank and I. Turan, Phys. Rev. D **74**, 073014 (2006).
[15] W. Fischler, S. Paban, and S. D. Thomas, Phys. Lett. B **289**, 373 (1992); S. M. Barr, Int. J. Mod. Phys. A **8**, 209 (1993); V. D. Barger, T. Falk, T. Han, J. Jiang, T. Li, and T. Plehn, Phys. Rev. D **64**, 056007 (2001); C. A. Baker *et al.*, Phys. Rev. Lett. **97**, 131801 (2006).
[16] D. A. Demir, O. Lebedev, K. A. Olive, M. Pospelov, and A. Ritz, Nucl. Phys. **B680**, 339 (2004); D. A. Demir and M. B. Voloshin, Phys. Rev. D **63**, 115011 (2001).
[17] F. Gabbiani, E. Gabrielli, A. Masiero, and L. Silvestrini, Nucl. Phys. **B477**, 321 (1996); M. Misiak, S. Pokorski, and J. Rosiek, Adv. Ser. Dir. High Energy Phys. **15**, 795 (1998); E. Lunghi, A. Masiero, I. Scimemi, and L. Silvestrini, Nucl. Phys. **B568**, 120 (2000); M. Ciuchini, E. Franco, A. Masiero, and L. Silvestrini, Phys. Rev. D **67**, 075016 (2003); **68**, 079901(E) (2003).
[18] D. Atwood, S. Bar-Shalom, G. Eilam, and A. Soni, Phys. Rep. **347**, 1 (2001).
[19] X. J. Bi and Y. B. Dai, Eur. Phys. J. C **12**, 125 (2000).
[20] S. Heinemeyer, W. Hollik, and G. Weiglein, Comput. Phys. Commun. **124**, 76 (2000); Eur. Phys. J. C **9**, 343 (1999); G. Degrassi, S. Heinemeyer, W. Hollik, P. Slavich, and G. Weiglein, Eur. Phys. J. C **28**, 133 (2003); T. Hahn, W. Hollik, S. Heinemeyer, and G. Weiglein, in *Proceedings of 2005 International Linear Collider Workshop (LCWS 2005), Stanford, California, 2005*, p. 0106; M. Frank, T. Hahn, S. Heinemeyer, W. Hollik, H. Rzehak, and G. Weiglein, J. High Energy Phys. 02 (2007) 047.
[21] A. Djouadi, J. Kalinowski, and P. M. Zerwas, Z. Phys. C **70**, 435 (1996).
[22] G. Passarino and M. J. G. Veltman, Nucl. Phys. **B160**, 151 (1979).
[23] R. E. Cutkosky, J. Math. Phys. (N.Y.) **1**, 429 (1960); G. 't Hooft and M. Veltman, *Diagrammar*, CERN Report No. CERN-73-09;M. E. Peskin and D. V. Schroeder, *An Introduction to Quantum Field Theory* (Addison-Wesley, Reading, MA, 1995).
[24] S. Bauberger and M. Bohm, Nucl. Phys. **B445**, 25 (1995); S. Bauberger, M. Bohm, G. Weiglein, F. A. Berends, and M. Buza, Nucl. Phys. B, Proc. Suppl. **37**, 95 (1994).
[25] G. Scharf, *Finite Quantum Electrodynamics: The Causal Approach* (Springer, Berlin, 1995).
[26] T. Hahn and M. Perez-Victoria, Comput. Phys. Commun. **118**, 153 (1999); T. Hahn, Nucl. Phys. B, Proc. Suppl. **89**, 231 (2000); Comput. Phys. Commun. **140**, 418 (2001); T. Hahn and C. Schappacher, Comput. Phys. Commun. **143**, 54 (2002).